RESEARCH ARTICLE

Artificial Neural Network-Based Modeling of Transient Bio-Convective Williamson Tri-Hybrid Nanofluid Flow with Gyrotactic Microorganisms over a Stretching Sheet

Abdul Hafeez[1], **Javed Khan**[2,*] **and Xiao Ying**[2]

[1] Department of Mathematics, The Islamia University of Bahawalpur, Bahawalpur 63100, Pakistan
[2] School of Mathematics and Computational Science, Xiangtan University, Xiangtan 411105, China

Abstract

In this paper, we study the unsteady magnetohydrodynamic (MHD) flow and the heat and mass transfer of a Williamson tri-hybrid nanofluid (THNF) composed of water and Al_2O_3, TiO_2 and Cu nanoparticles over a stretching sheet. The model incorporates thermal radiation, activation energy, chemical reaction, a heat source and the bioconvection of motile gyrotactic microorganisms. An artificial neural network (ANN) is employed for the predictive modeling of such THNF flows under these combined effects. Similarity transformations reduce the governing nonlinear partial differential equations (PDEs) to coupled ordinary differential equations (ODEs), which are solved numerically with a boundary-value-problem solver (SciPy `solve_bvp`). A feed-forward ANN is trained on the numerical dataset and validated through regression analysis, training convergence, comparison of numerical and predicted data, and error analysis, which results in an ANN with excellent predictive accuracy. The results show that the magnetic field, thermal radiation, Eckert number and heat source increase the temperature field, whereas the Williamson and unsteadiness parameters decrease the velocity profile. The concentration increases with the activation energy, whereas a stronger chemical reaction and a larger Schmidt number lower the concentration profile. Furthermore, the skin-friction coefficient, Nusselt number, Sherwood number and motile-microorganism density number are evaluated over a range of physical parameters. The proposed ANN-assisted framework is an efficient and reliable tool for analyzing and optimizing advanced THNF-based thermal systems.

Keywords: tri-hybrid nanofluid, williamson fluid, neural network prediction, stretching sheet, gyrotactic microorganisms, activation energy, transient flow.

Submitted: 27 June 2026
Revised: 07 September 2026
Accepted: 21 September 2026
Published: 06 October 2026

Vol. 2, **No.** 4, 2026.
10.62762/JAM.2026.618998

***Corresponding author:**
Javed Khan
jkhan8303974@gmail.com

Citation
Hafeez, A., Khan, J., & Ying, X. (2026). Artificial Neural Network-Based Modeling of Transient Bio-Convective Williamson Tri-Hybrid Nanofluid Flow with Gyrotactic Microorganisms over a Stretching Sheet. *ICCK Journal of Applied Mathematics*, 2(4), 266–282.

© 2026 by the Authors. Published by Institute of Central Computation and Knowledge. This is an open access article under the CC BY license (https://creativecommons.org/licenses/by/4.0/).

Table 1. Nomenclature of physical parameters.

Symbol	Description	Unit	Symbol	Description	Unit
u, v	Velocity components in the x and y directions	$\mathrm{m\,s^{-1}}$	ρ	Fluid density	$\mathrm{kg\,m^{-3}}$
x, y	Cartesian coordinates along and normal to the surface	m	C_p	Specific heat capacity	$\mathrm{J\,kg^{-1}\,K^{-1}}$
t	Time	s	D_B	Brownian diffusion coefficient	$\mathrm{m^2\,s^{-1}}$
T	Fluid temperature	K	D_T	Thermophoretic diffusion coefficient	$\mathrm{m^2\,s^{-1}}$
T_w	Wall temperature	K	D_m	Microorganism diffusivity	$\mathrm{m^2\,s^{-1}}$
T_∞	Ambient temperature	K	W_c	Maximum swimming speed of microorganisms	$\mathrm{m\,s^{-1}}$
C	Nanoparticle concentration	$\mathrm{kg\,m^{-3}}$	Q_0	Heat source coefficient	$\mathrm{W\,m^{-3}\,K^{-1}}$
C_w	Wall nanoparticle concentration	$\mathrm{kg\,m^{-3}}$	g	Gravitational acceleration	$\mathrm{m\,s^{-2}}$
C_∞	Ambient nanoparticle concentration	$\mathrm{kg\,m^{-3}}$	β_T	Thermal expansion coefficient	$\mathrm{K^{-1}}$
N	Density of motile microorganisms	$\mathrm{m^{-3}}$	β_C	Solutal expansion coefficient	$\mathrm{m^3\,kg^{-1}}$
N_w	Wall microorganism density	$\mathrm{m^{-3}}$	β_n	Microorganism density coefficient	$\mathrm{m^3}$
N_∞	Ambient microorganism density	$\mathrm{m^{-3}}$	a	Stretching rate constant	$\mathrm{s^{-1}}$
U_w	Stretching velocity of the sheet	$\mathrm{m\,s^{-1}}$	b	Chemotaxis constant	m
B_0	Magnetic field strength	T	c	Unsteadiness constant	$\mathrm{s^{-1}}$
K	Permeability of the porous medium	$\mathrm{m^2}$	Γ	Williamson time constant	s
k_r	Chemical reaction rate constant	$\mathrm{s^{-1}}$	τ	Ratio of nanoparticle to base-fluid heat capacity	–
E_a	Activation energy	J	n	Fitted rate constant (exponent)	–
κ	Boltzmann constant	$\mathrm{J\,K^{-1}}$	σ^*	Stefan–Boltzmann constant	$\mathrm{W\,m^{-2}\,K^{-4}}$
k	Thermal conductivity	$\mathrm{W\,m^{-1}\,K^{-1}}$	k^*	Rosseland mean absorption coefficient	$\mathrm{m^{-1}}$
q_r	Radiative heat flux	$\mathrm{W\,m^{-2}}$	ϕ_1, ϕ_2, ϕ_3	Volume fractions of Al_2O_3, TiO_2 and Cu	–
σ	Electrical conductivity	$\mathrm{S\,m^{-1}}$	f, nf	Subscripts: base fluid, nanofluid	–
μ	Dynamic viscosity	$\mathrm{kg\,m^{-1}\,s^{-1}}$	hnf, $thnf$	Subscripts: hybrid, tri-hybrid nanofluid	–
ν	Kinematic viscosity	$\mathrm{m^2\,s^{-1}}$			

1 Introduction

Hybrid and tri-hybrid nanofluids (THNFs) have received considerable attention because their thermal conductivity and heat transfer performance are better than those of conventional nanofluids. A THNF is obtained by dispersing three different nanoparticles in a single base fluid, which significantly improves its thermal capability and makes such fluids suitable for advanced thermal engineering applications (see Table 1 for the nomenclature). Xuan et al. [1] investigated the thermo-economic performance and sensitivity analysis of ternary hybrid nanofluids and demonstrated that the synergistic combination of multiple nanoparticles yields significant enhancements in thermal conductivity and overall heat transfer performance. The preparation of hybrid and tri-hybrid nanofluids is illustrated in Figure 1. Machine learning methods are increasingly used to predict complex transport phenomena in nanofluids. Imran et al. [2] applied a Bayesian-regularization neural network to the thermal analysis of THNF flow over a stretched sheet, and Hussain et al. [3] used an artificial neural network (ANN) to model a blood-based THNF. Keerthiga and Reddy [4] compared several neural networks for the unsteady MHD Casson THNF flow over a rotating sphere, Faisal et al. [5] combined an ANN with Levenberg–Marquardt optimization to examine the influence of nanolayer morphology on a magnetized THNF, and Jalili et al. [6] used a deep ANN to predict the thermal and flow fields of a magnetized Boger-micropolar THNF. Butt et al. [7] employed a radial basis kernel harmony neural

network to analyze MHD Williamson nanofluid flow with thermal radiation and chemical reaction, demonstrating the effectiveness of evolutionary neural network approaches for non-Newtonian nanofluid systems. However, most of these investigations consider comparatively simple flow configurations and do not include the combined effects of an unsteady Williamson fluid, activation energy, chemical reaction and gyrotactic microorganisms together with a detailed ANN validation.

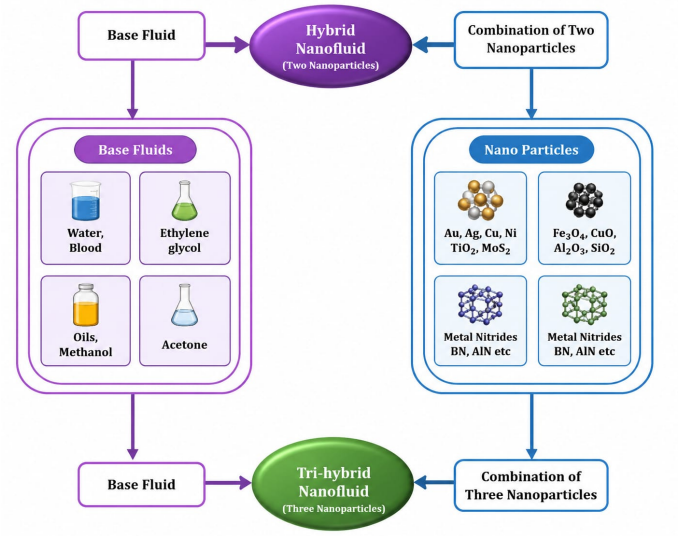

Figure 1. Production of the hybrid nanofluid and the tri-hybrid nanofluid.

The Williamson model is widely applied to shear-thinning non-Newtonian fluids encountered in polymer processing, coating processes, biomedical engineering and industrial manufacturing. Unlike a Newtonian fluid, a Williamson fluid exhibits a viscosity that decreases with increasing shear rate, and the model describes many real fluids used in practice. Williamson fluid flow has been examined under various physical conditions. Sankari et al. [8] examined MHD Williamson nanofluid flow over a porous exponentially stretching sheet with bioconvective fluxes, providing insights into the interplay between magnetic effects, porous resistance and bioconvection in Williamson fluid systems, and Sankari et al. [9] derived an analytical solution for MHD bioconvection Williamson nanofluid flow over an exponentially stretching sheet incorporating viscous dissipation and gyrotactic microorganisms, highlighting the coupled roles of bioconvection and Williamson rheology in boundary-layer transport. Chakradhar et al. [10] examined the MHD effect on the peristaltic motion of a Williamson fluid in a porous channel with suction and injection. Divya et al. [11] considered mixed convection and a heat sink/source for a Williamson fluid bounded by a nonlinear curved surface, and Kumar et al. [12] optimized the thermal characteristics of Williamson fluid flow through a microchannel under the Hall effect using response surface methodology, further demonstrating the broad applicability of the Williamson fluid model in thermal engineering optimization. Nevertheless, unsteady Williamson hybrid nanofluids with activation energy, bioconvection and machine-learning assistance have not yet been investigated extensively.

The bioconvection generated by gyrotactic microorganisms is significant for the stability of nanofluid systems, for preventing nanoparticle sedimentation and for improving heat and mass transfer, which has led to a growing interest in bioconvective transport in recent years. Waqas et al. [13] studied bioconvection in a Sutterby nanofluid between two rotating disks, and Ahmad et al. [14] analyzed the influence of activation energy and bioconvection on the thin-film flow of an Oldroyd-B fluid. Ben Hamida et al. [15], Madkhali et al. [16], Arif and Nawaz [17], Sarma and Sarma [18] and Hussain et al. [19] investigated bioconvection with gyrotactic microorganisms in other fluid models and magnetic-field configurations. However, the combination of gyrotactic microorganisms with an unsteady Williamson THNF, activation energy and ANN-based validation has received much less attention.

Activation energy and chemical reaction strongly influence species diffusion, and hence the heat and mass transfer in chemically reacting nanofluids; including them gives a more realistic representation of industrial and chemical engineering processes. Panda et al. [20] carried out an optimization and sensitivity analysis of the effect of Arrhenius activation energy on a two-phase nanofluid flow, and Raju et al. [21] examined the effects of reversible and irreversible chemical reactions and activation energy on convective Maxwell fluid flow in a porous medium, demonstrating how activation energy governs species transport in chemically reactive non-Newtonian flow systems. Varatharaj et al. [22] and Ullah et al. [23] included the activation energy in Carreau nanofluid and ternary hybrid nanofluid models, respectively, by means of numerical simulation, while Anwar et al. [24] and Ayman-Mursaleen et al. [25] applied recurrent and deep neural networks, respectively, to hybrid nanofluid flows with activation energy. However, these studies do not address the simultaneous effects

of an unsteady Williamson THNF, bioconvection and a porous medium together with a comprehensive machine-learning validation.

1.1 Research gap and motivation

Much research has been carried out on non-Newtonian nanofluid flows. However, to the best of the authors' knowledge, no study has combined all of the following physical effects in one model: unsteady Williamson fluid behavior, a magnetic field, a porous medium, thermal radiation, a heat source, activation energy, chemical reaction, Brownian motion, thermophoresis and gyrotactic microorganisms. How these factors influence each other is still not well understood.

Similarly, recent machine learning studies in this area have mostly focused on achieving a high prediction accuracy, and the comparison with numerical solutions through regression analysis, error checking and performance evaluation is not always reported in detail, which makes it difficult to judge the reliability of the predictions.

To address these issues, we develop a complete mathematical model that includes all the above physical mechanisms, together with a machine learning approach that is validated through detailed error and performance analyses against numerical solutions. In this way, we aim to provide accurate and trustworthy results for complex nanofluid flow problems.

2 Novelty and Contribution

In the present study, a complete mathematical model of the unsteady Williamson tri-hybrid nanofluid flow over a stretching sheet is developed for analyzing the heat and mass transfer processes involved. Unlike previous studies, the proposed model covers all the aforementioned effects in a single formulation. The governing equations are transformed, solved numerically and independently verified by a feed-forward ANN. The results predicted by the ANN are in very good agreement with the numerical solution; for the profile examined in Section 6.6, the absolute error is of the order of 10^{-6}, which supports the accuracy and robustness of the proposed computational approach. The main contributions of the present study are:

- Formulation of an unsteady Williamson THNF model with multiple coupled physical effects: magnetohydrodynamics, a porous medium, thermal radiation, heat generation, activation energy, chemical reaction, Brownian diffusion, thermophoresis and bioconvection due to gyrotactic microorganisms.
- Validation of the numerical solutions with a feed-forward ANN.
- Full validation of the ANN by regression, training loss, error histogram and absolute error.
- Development of a stable computational solution of complex nonlinear transport phenomena.

3 Research Questions

The following research questions guide this study:

- What are the effects of Al_2O_3, TiO_2 and Cu nanoparticles in a Williamson THNF on the unsteady boundary-layer flow over a stretching sheet?
- How do the activation energy and the chemical reaction influence the concentration distribution and the mass transport of the nanofluid system?
- How does a heat source change the thermal behavior and the temperature profile in the boundary layer?
- How does the bioconvection of motile microorganisms act on the flow and on the density distribution of the microorganisms?
- How well does a feed-forward ANN predict the nonlinear velocity, temperature, concentration and microorganism profiles compared with the numerical solutions?
- How do the skin-friction coefficient, Nusselt number, Sherwood number and microorganism density number change when the physical parameters are varied?

4 Mathematical Modeling

Consider the unsteady two-dimensional flow of a Williamson THNF over a continuously stretching sheet embedded in a saturated porous medium containing gyrotactic microorganisms. The sheet moves with velocity $U_w(x,t) = ax/(1-ct)$, where $a > 0$ is the stretching rate and c is the unsteadiness constant; the formulation is valid for $ct < 1$. A uniform transverse magnetic field B_0 is imposed normal to the sheet, giving rise to magnetohydrodynamic (MHD) effects. The model accounts for the shear-thinning rheology of the Williamson fluid, the resistance of the porous medium and the temporal changes in the flow field, and is applicable to a wide range

of engineering, industrial and biomedical problems. Gyrotactic microorganisms are suspended in the fluid to promote bioconvection and thereby improve nanoparticle dispersion, mass transport and stability. Brownian motion, thermophoresis, activation energy and chemical reaction are included to describe the thermal and concentration transport mechanisms. The working fluid is a water-based THNF containing the three nanoparticles Al_2O_3, TiO_2 and Cu, whose synergistic effect significantly enhances the thermal conductivity and heat transfer properties of the fluid. The physical configuration is shown in Figure 2.

4.1 Governing equations

The governing equations of the model, namely the continuity, momentum, energy, concentration and gyrotactic-microorganism density equations, are given below, following Rehman et al. [26].

Continuity equation:

$$\frac{\partial u}{\partial x} + \frac{\partial v}{\partial y} = 0, \tag{1}$$

Momentum equation:

$$\begin{aligned} &\frac{\partial u}{\partial t} + u\frac{\partial u}{\partial x} + v\frac{\partial u}{\partial y} \\ &\quad = \nu_{thnf}\frac{\partial^2 u}{\partial y^2} + \sqrt{2}\,\Gamma\,\nu_{thnf}\frac{\partial u}{\partial y}\frac{\partial^2 u}{\partial y^2} \\ &\qquad - \frac{\sigma_{thnf}B_0^2}{\rho_{thnf}}u - \frac{\mu_{thnf}}{\rho_{thnf}K}u \\ &\qquad + g\big[\beta_T(T-T_\infty) + \beta_C(C-C_\infty) \\ &\qquad\quad + \beta_n(N-N_\infty)\big], \end{aligned} \tag{2}$$

Energy equation:

$$\begin{aligned} &\frac{\partial T}{\partial t} + u\frac{\partial T}{\partial x} + v\frac{\partial T}{\partial y} \\ &\quad = \frac{k_{thnf}}{(\rho C_p)_{thnf}}\frac{\partial^2 T}{\partial y^2} - \frac{1}{(\rho C_p)_{thnf}}\frac{\partial q_r}{\partial y} \\ &\qquad + \frac{\sigma_{thnf}B_0^2}{(\rho C_p)_{thnf}}u^2 + \frac{\mu_{thnf}}{(\rho C_p)_{thnf}}\left(\frac{\partial u}{\partial y}\right)^2 \\ &\qquad + \tau\left[D_B\frac{\partial C}{\partial y}\frac{\partial T}{\partial y} + \frac{D_T}{T_\infty}\left(\frac{\partial T}{\partial y}\right)^2\right] \\ &\qquad + \frac{Q_0}{(\rho C_p)_{thnf}}(T-T_\infty), \end{aligned} \tag{3}$$

Concentration equation:

$$\begin{aligned} &\frac{\partial C}{\partial t} + u\frac{\partial C}{\partial x} + v\frac{\partial C}{\partial y} = D_B\frac{\partial^2 C}{\partial y^2} + \frac{D_T}{T_\infty}\frac{\partial^2 T}{\partial y^2} \\ &\qquad - k_r(C-C_\infty)\left(\frac{T}{T_\infty}\right)^n \exp\left(\frac{-E_a}{\kappa T}\right), \end{aligned} \tag{4}$$

Gyrotactic microorganism density equation:

$$\frac{\partial N}{\partial t} + u\frac{\partial N}{\partial x} + v\frac{\partial N}{\partial y} = D_m\frac{\partial^2 N}{\partial y^2} - bW_c\frac{\partial}{\partial y}\left(N\frac{\partial C}{\partial y}\right). \tag{5}$$

4.2 Thermal radiation

The radiative heat flux q_r is obtained from the Rosseland approximation [27]:

$$q_r = -\frac{4\sigma^*}{3k^*}\frac{\partial T^4}{\partial y}, \qquad T^4 \approx 4T_\infty^3 T - 3T_\infty^4,$$

$$q_r = -\frac{16\sigma^* T_\infty^3}{3k^*}\frac{\partial T}{\partial y},$$

where $\sigma^* \cong 5.67 \times 10^{-8}\ \mathrm{W\,m^{-2}\,K^{-4}}$ is the Stefan–Boltzmann constant and k^* is the Rosseland mean absorption coefficient.

4.3 Boundary conditions

The boundary conditions of the model are as follows:

$$\left.\begin{aligned} &u = \frac{ax}{1-ct}, \quad v = 0, \quad T = T_w, \\ &C = C_w, \quad N = N_w \quad \text{at } y = 0, \\ &u \to 0, \quad T \to T_\infty, \quad C \to C_\infty, \\ &N \to N_\infty \quad \text{as } y \to \infty. \end{aligned}\right\} \tag{6}$$

4.4 Similarity transformations

The similarity transformations that convert the PDEs into ODEs are taken from Ouyang et al. [28]:

$$\left.\begin{aligned} &\eta = \sqrt{\frac{a}{\nu_f(1-ct)}}\,y, \qquad u = \frac{ax}{1-ct}f'(\eta), \\ &v = -\sqrt{\frac{a\nu_f}{1-ct}}\,f(\eta), \qquad \theta(\eta) = \frac{T-T_\infty}{T_w-T_\infty}, \\ &\phi(\eta) = \frac{C-C_\infty}{C_w-C_\infty}, \qquad \chi(\eta) = \frac{N-N_\infty}{N_w-N_\infty}. \end{aligned}\right\} \tag{7}$$

4.5 ODE system

Substituting the similarity transformations of Eq. (7) into the governing equations (1)–(5) and the boundary conditions (6) yields the nonlinear ordinary differential equations (8)–(11) with the boundary conditions (12).

Momentum equation:

$$\begin{aligned} &B_1 f''' + B_1\,We\,f''f''' + B_2(ff'' - f'^2) \\ &\quad - B_2A\left(f' + \frac{\eta}{2}f''\right) - B_4Mf' - B_1K_pf' \\ &\quad + B_2\lambda_T\theta + B_2\lambda_C\phi \\ &\quad + B_2\lambda_n\chi = 0, \end{aligned} \tag{8}$$

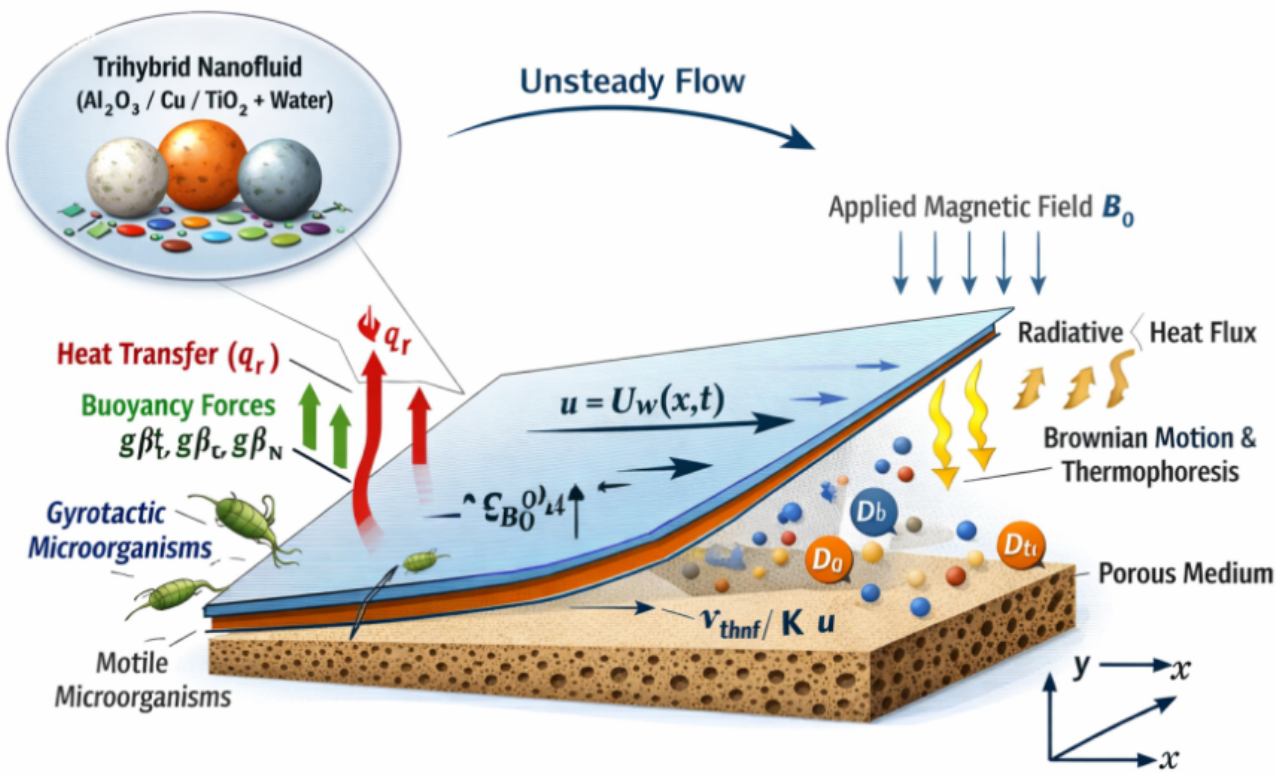

Figure 2. Physical model of the problem.

Energy equation:

$$\frac{B_5}{Pr}\left(1+\frac{4}{3}Rd\right)\theta''+B_3 f\theta'-B_3 A\left(\theta+\frac{\eta}{2}\theta'\right)+Nb\,\phi'\theta' + Nt\,\theta'^2+B_1 Ec\,f''^2+Q\theta+B_4 M\,Ec\,f'^2=0, \tag{9}$$

Concentration equation:

$$\phi''+Sc\,f\phi'-Sc\,A\left(\phi+\frac{\eta}{2}\phi'\right)+\frac{Nt}{Nb}\theta'' - Sc\,Cr\,(1+\delta\theta)^n\phi\exp\left(-\frac{E}{1+\delta\theta}\right)=0, \tag{10}$$

Gyrotactic microorganism density equation:

$$\chi''+Sm\,f\chi'-Sm\,A\left(\chi+\frac{\eta}{2}\chi'\right)-Pe\,(\chi\phi')'=0. \tag{11}$$

Boundary conditions:

$$\left.\begin{aligned} &f'(0)=1, \quad f(0)=0, \quad \theta(0)=1,\\ &\phi(0)=1, \quad \chi(0)=1,\\ &f'(\infty)\to 0, \quad \theta(\infty)\to 0,\\ &\phi(\infty)\to 0, \quad \chi(\infty)\to 0. \end{aligned}\right\} \tag{12}$$

4.6 Dimensionless parameters

The dimensionless parameters appearing in Eqs. (8)–(11) are defined in Table 2.

4.7 Engineering quantities

The skin-friction coefficient Cf_x, Nusselt number Nu_x, Sherwood number Sh_x and density number of motile microorganisms Nn_x are defined as

$$\left.\begin{aligned} Cf_x&=\frac{\tau_w}{\rho_f U_w^2}, \qquad Nu_x=\frac{xq_w}{k_f(T_w-T_\infty)},\\ Sh_x&=\frac{xq_B}{D_B(C_w-C_\infty)}, \qquad Nn_x=\frac{xq_n}{D_m(N_w-N_\infty)}, \end{aligned}\right\} \tag{13}$$

where the wall shear stress, heat flux, mass flux and microorganism flux are $\tau_w=\mu_{thnf}\,(\partial u/\partial y)_{y=0}$, $q_w=-k_{thnf}\,(\partial T/\partial y)_{y=0}$, $q_B=-D_B\,(\partial C/\partial y)_{y=0}$ and $q_n=-D_m\,(\partial N/\partial y)_{y=0}$, respectively. In non-dimensional form these quantities become

$$\left.\begin{aligned} Cf_x Re_x^{1/2}&=B_1 f''(0), \quad Nu_x Re_x^{-1/2}=-B_5\theta'(0),\\ Sh_x Re_x^{-1/2}&=-\phi'(0), \quad Nn_x Re_x^{-1/2}=-\chi'(0), \end{aligned}\right\} \tag{14}$$

where $Re_x=U_w x/\nu_f$ is the local Reynolds number.

4.8 Machine learning formulation

In the present study, a machine learning framework based on a feed-forward artificial neural network (ANN) is added to extend the predictive capability and to validate the numerical results. The network learns the nonlinear relationship between the governing parameters and the solution profiles produced by

Table 2. Dimensionless parameters of the transformed problem.

Symbol	Description	Symbol	Description
$A = \frac{c}{a}$	Unsteadiness parameter	$M = \frac{(1-ct)\sigma_f B_0^2}{\rho_f a}$	Magnetic parameter
$Pr = \frac{\nu_f}{\alpha_f} = \frac{(\mu C_p)_f}{k_f}$	Prandtl number	$Sc = \frac{\nu_f}{D_B}$	Schmidt number
$K_p = \frac{\nu_f(1-ct)}{Ka}$	Porosity parameter	$We = \Gamma x\sqrt{\frac{2a^3}{\nu_f(1-ct)^3}}$	Williamson parameter
$Cr = \frac{k_r(1-ct)}{a}$	Chemical reaction parameter	$Ec = \frac{U_w^2}{(C_p)_f(T_w - T_\infty)}$	Eckert number
$Rd = \frac{4\sigma^* T_\infty^3}{k^* k_{thnf}}$	Radiation parameter	$Nb = \frac{\tau D_B(C_w - C_\infty)}{\nu_f}$	Brownian motion parameter
$Q = \frac{Q_0(1-ct)}{(\rho C_p)_f\, a}$	Heat source parameter	$Nt = \frac{\tau D_T(T_w - T_\infty)}{\nu_f T_\infty}$	Thermophoresis parameter
$E = \frac{E_a}{\kappa T_\infty}$	Activation energy parameter	$Sm = \frac{\nu_f}{D_m}$	Bioconvection Schmidt number
$\delta = \frac{T_w - T_\infty}{T_\infty}$	Temperature difference parameter	$Pe = \frac{bW_c(N_w - N_\infty)}{D_m}$	Bioconvection Peclet number
$\lambda_T = \frac{g\beta_T(T_w - T_\infty)x}{U_w^2}$	Thermal buoyancy parameter	$\lambda_C = \frac{g\beta_C(C_w - C_\infty)x}{U_w^2}$	Solutal buoyancy parameter
$\lambda_n = \frac{g\beta_n(N_w - N_\infty)x}{U_w^2}$	Bioconvection buoyancy parameter	$Re_x = \frac{U_w x}{\nu_f}$	Local Reynolds number
$B_1 = \frac{\mu_{thnf}}{\mu_f}$	Dynamic viscosity ratio	$B_3 = \frac{(\rho C_p)_{thnf}}{(\rho C_p)_f}$	Heat capacity ratio
$B_2 = \frac{\rho_{thnf}}{\rho_f}$	Density ratio	$B_4 = \frac{\sigma_{thnf}}{\sigma_f}$	Electrical conductivity ratio
$B_5 = \frac{k_{thnf}}{k_f}$	Thermal conductivity ratio		

the numerical scheme. The input layer contains the physical parameters, including the unsteadiness parameter A and the nanoparticle volume fraction ϕ_3, together with the similarity variable η. The output layer returns the dependent variables of interest: the velocity $f'(\eta)$, temperature $\theta(\eta)$, concentration $\phi(\eta)$ and density of motile microorganisms $\chi(\eta)$. The training data are obtained by varying the parameter A over a range of values; for each parametric condition, the numerical solution computed by the boundary-value-problem solver forms the basis of the training dataset.

The network consists of two hidden layers with 64 neurons each and uses the tanh activation function to capture the highly nonlinear behavior of the system. The model is trained with the Adam optimization algorithm and the mean squared error (MSE) loss. Training progressively minimizes the difference between the predicted and the numerical profiles so that the network approximates the solution profiles with a small error. After training, the network is checked against the numerical results by comparison plots, error analysis and regression analysis. The agreement between the predicted and numerical solutions supports the reliability of the machine-learning approach and its generalization capability. The combination of numerical and data-driven modeling offers a powerful, efficient and reliable way of simulating complex non-Newtonian nanofluid flows. The structure of the data-driven model is shown in Figure 3.

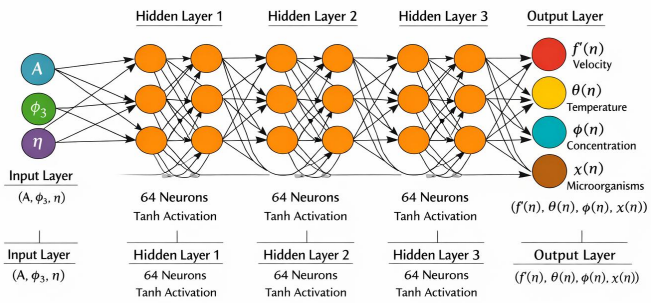

Figure 3. Schematic representation of the data-driven (ANN) model.

4.9 Thermo-physical properties

The thermo-physical properties of the nanoparticles and the base fluid are listed in Table 3, and the correlations used for the THNF are given in Table 4. Following Guedri et al. [29], the Maxwell–Garnett model for thermal conductivity and electrical conductivity and the Brinkman model for viscosity are applied sequentially across the three nanoparticle species to obtain the effective tri-hybrid nanofluid properties.

Table 3. Thermo-physical characteristics of the nanoparticles and the base fluid [29].

Material	c_p $(\mathrm{J\,kg^{-1}\,K^{-1}})$	ρ $(\mathrm{kg\,m^{-3}})$	k $(\mathrm{W\,m^{-1}\,K^{-1}})$	σ $(\mathrm{S\,m^{-1}})$
H_2O	4184	997	0.613	1.4×10^{-7}
Al_2O_3	765	3970	40	1.2×10^{-5}
TiO_2	692	4250	8.5	2.8×10^{-6}
Cu	385	8933	401	1.1×10^{-5}

5 Methodology

In the present study, the two-dimensional unsteady MHD flow of a Williamson THNF over a stretching sheet in a porous medium is studied. Suitable similarity transformations convert the governing continuity, momentum, energy, concentration and microorganism-density equations into nonlinear ordinary differential equations. The resulting boundary value problem is solved numerically in Python with the SciPy `solve_bvp` solver. A feed-forward ANN is then developed and trained on the numerical dataset to validate the numerical solutions. The ANN has an input layer, two hidden layers of 64 neurons each with the tanh activation function, and an output layer. The network is trained with the Adam optimizer and a mean squared error (MSE) loss function. The accuracy of the trained ANN is assessed through the regression plot, the training-loss curve, the histogram of prediction errors and the absolute error. Lastly, the effects of the governing parameters on the flow behavior and on the engineering quantities are analyzed. The overall procedure is summarized in Figure 4.

6 Results and Discussion

In this section, the effects of thermophoresis, activation energy, the porous medium, the magnetic field and Joule heating on the THNF flow over a stretching sheet are investigated. The THNF consists of Al_2O_3, TiO_2 and Cu nanoparticles dispersed in a water-based Williamson fluid. The governing PDEs are converted

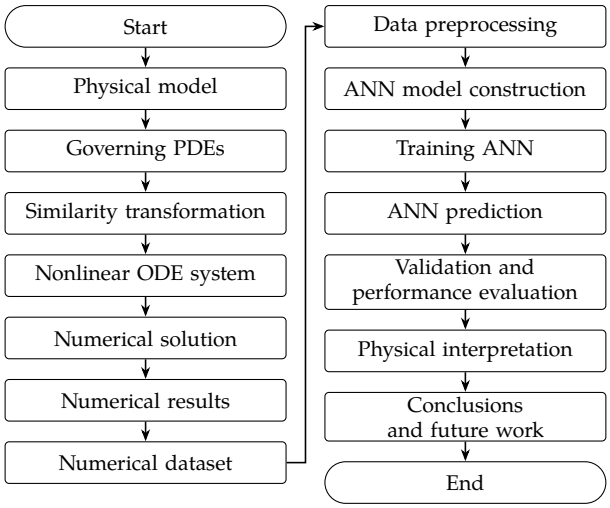

Figure 4. Procedure followed in the present study.

into ODEs by the similarity transformations and solved with the SciPy `solve_bvp` solver, as described in the Methodology section. In every figure the results for the tri-hybrid nanofluid (Thnf) are plotted together with those of a hybrid nanofluid (Hnf) for comparison. The influence of the governing parameters on the velocity, temperature, concentration and gyrotactic-microorganism density profiles is discussed below.

6.1 Velocity profile $f'(\eta)$

The effects of the Williamson parameter We, the magnetic parameter M, the unsteadiness parameter A and the porosity parameter K_p on the velocity profile $f'(\eta)$ are shown in Figures 5–8, respectively. The velocity decreases as each of these four parameters increases, but each parameter acts through a different physical mechanism. A higher Williamson parameter We strengthens the non-Newtonian behavior of the fluid and increases its resistance to motion, which reduces the thickness of the momentum boundary layer. Likewise, a larger magnetic parameter M produces a stronger Lorentz force that opposes the flow and reduces the velocity. As the unsteadiness parameter A increases, momentum transport is reduced because the time-dependent disturbances suppress the development of the boundary layer, which lowers the fluid velocity. A higher porosity parameter K_p corresponds to a lower permeability of the medium and therefore to a larger drag force, which further suppresses the velocity field. These observations show that the non-Newtonian behavior, magnetic braking, flow unsteadiness and porous-medium resistance all play a key role in controlling momentum transport over the stretching

Table 4. Correlations for the thermo-physical properties of the tri-hybrid nanofluid [29]. Subscripts 1, 2 and 3 denote Al_2O_3, TiO_2 and Cu, respectively; B_4 and B_5 are the products of the three listed ratios.

Property	Correlation
$B_1 = \dfrac{\mu_{thnf}}{\mu_f}$	$(1-\phi_3)^{-2.5}(1-\phi_2)^{-2.5}(1-\phi_1)^{-2.5}$
$B_2 = \dfrac{\rho_{thnf}}{\rho_f}$	$(1-\phi_3)\left[(1-\phi_2)\left\{(1-\phi_1)+\phi_1\dfrac{\rho_1}{\rho_f}\right\}+\phi_2\dfrac{\rho_2}{\rho_f}\right]+\phi_3\dfrac{\rho_3}{\rho_f}$
$B_3 = \dfrac{(\rho C_p)_{thnf}}{(\rho C_p)_f}$	$(1-\phi_3)\left[(1-\phi_2)\left\{(1-\phi_1)+\phi_1\dfrac{(\rho C_p)_1}{(\rho C_p)_f}\right\}+\phi_2\dfrac{(\rho C_p)_2}{(\rho C_p)_f}\right]+\phi_3\dfrac{(\rho C_p)_3}{(\rho C_p)_f}$
$B_4 = \dfrac{\sigma_{thnf}}{\sigma_f}$	$\dfrac{\sigma_{nf}}{\sigma_f} = \dfrac{\sigma_1+2\sigma_f-2\phi_1(\sigma_f-\sigma_1)}{\sigma_1+2\sigma_f+\phi_1(\sigma_f-\sigma_1)}, \quad \dfrac{\sigma_{hnf}}{\sigma_{nf}} = \dfrac{\sigma_2+2\sigma_{nf}-2\phi_2(\sigma_{nf}-\sigma_2)}{\sigma_2+2\sigma_{nf}+\phi_2(\sigma_{nf}-\sigma_2)},$
	$\dfrac{\sigma_{thnf}}{\sigma_{hnf}} = \dfrac{\sigma_3+2\sigma_{hnf}-2\phi_3(\sigma_{hnf}-\sigma_3)}{\sigma_3+2\sigma_{hnf}+\phi_3(\sigma_{hnf}-\sigma_3)}$
$B_5 = \dfrac{k_{thnf}}{k_f}$	$\dfrac{k_{nf}}{k_f} = \dfrac{k_1+2k_f-2\phi_1(k_f-k_1)}{k_1+2k_f+\phi_1(k_f-k_1)}, \quad \dfrac{k_{hnf}}{k_{nf}} = \dfrac{k_2+2k_{nf}-2\phi_2(k_{nf}-k_2)}{k_2+2k_{nf}+\phi_2(k_{nf}-k_2)},$
	$\dfrac{k_{thnf}}{k_{hnf}} = \dfrac{k_3+2k_{hnf}-2\phi_3(k_{hnf}-k_3)}{k_3+2k_{hnf}+\phi_3(k_{hnf}-k_3)}$

sheet.

6.2 Temperature profile $\theta(\eta)$

The effects of the magnetic parameter M, unsteadiness parameter A, radiation parameter Rd, Eckert number Ec and heat source parameter Q on the temperature distribution $\theta(\eta)$ are shown in Figures 9–13. The magnetic parameter, radiation parameter, Eckert number and heat source parameter raise the temperature profile, whereas the unsteadiness parameter lowers it. A larger magnetic parameter produces a stronger Lorentz force that opposes the flow and heats the fluid through Joule heating, which thickens the thermal boundary layer. Similarly, as the radiation parameter increases, more thermal energy is supplied to the fluid, which raises the temperature distribution and enhances thermal diffusion. A higher Eckert number increases viscous dissipation, which converts more mechanical energy into internal energy and hence raises the fluid temperature. Furthermore, the heat source adds heat to the system and produces a stronger thermal field throughout the boundary layer. A larger unsteadiness parameter leaves less time for heat diffusion and therefore reduces the temperature profile and the thickness of the thermal boundary layer.

6.3 Concentration profile $\phi(\eta)$

The influence of the unsteadiness parameter A, activation energy parameter E, Schmidt number Sc and chemical reaction parameter Cr on the concentration profile $\phi(\eta)$ is shown in Figures 14–17, respectively. The concentration decreases as the unsteadiness parameter, Schmidt number and chemical reaction parameter increase, whereas it increases with the activation energy. A larger unsteadiness parameter enhances the transient nature of the flow, which leaves less time for species diffusion and reduces the thickness of the concentration boundary layer. When the activation energy is higher, the chemical reaction proceeds more slowly because more energy is required to initiate it; more species therefore remain and the concentration within the boundary layer is higher. As the Schmidt number increases, the mass diffusivity decreases, which weakens species transport and reduces both the thickness of the concentration boundary layer and the concentration profile. Similarly, as the chemical reaction parameter increases, the diffusing species is consumed more rapidly, which steepens the concentration gradient across the boundary layer. These results indicate that the activation energy raises the species concentration in the boundary layer by

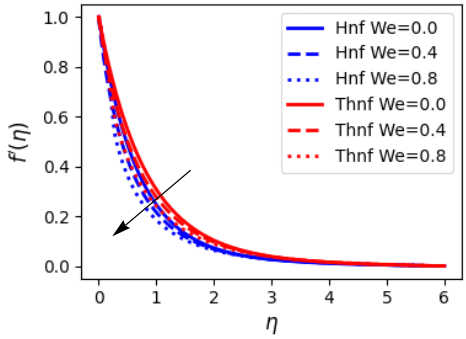

Figure 5. Influence of the Williamson parameter We on the velocity profile $f'(\eta)$.

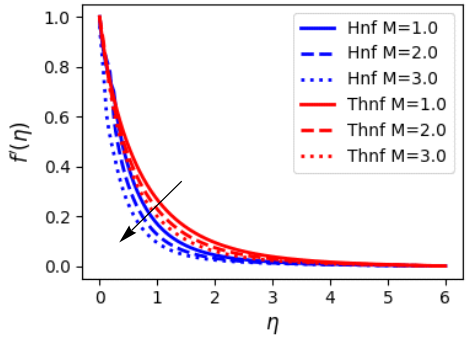

Figure 6. Influence of the magnetic parameter M on the velocity profile $f'(\eta)$.

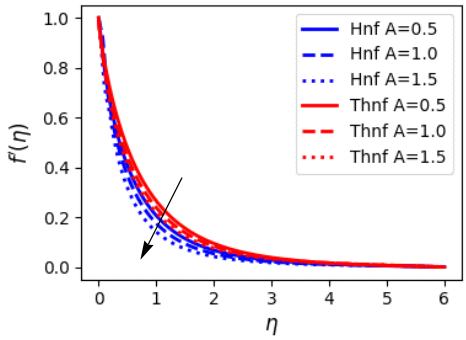

Figure 7. Influence of the unsteadiness parameter A on the velocity profile $f'(\eta)$.

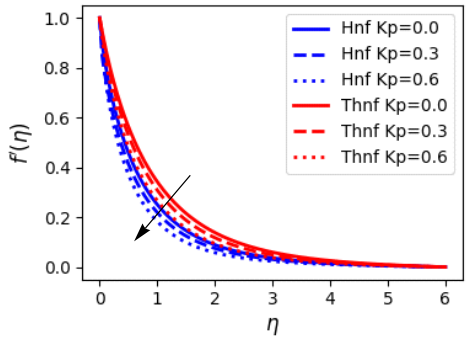

Figure 8. Influence of the porosity parameter K_p on the velocity profile $f'(\eta)$.

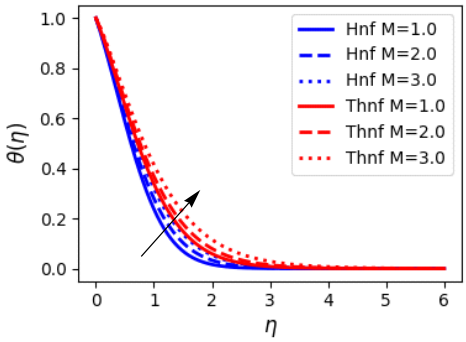

Figure 9. Influence of the magnetic parameter M on the temperature profile $\theta(\eta)$.

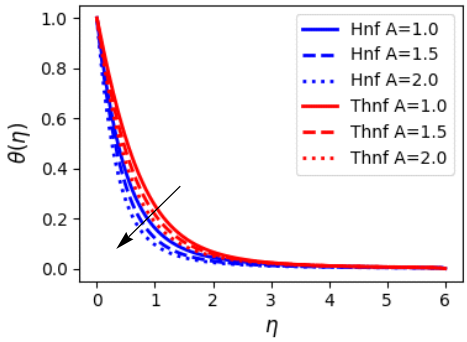

Figure 10. Influence of the unsteadiness parameter A on the temperature profile $\theta(\eta)$.

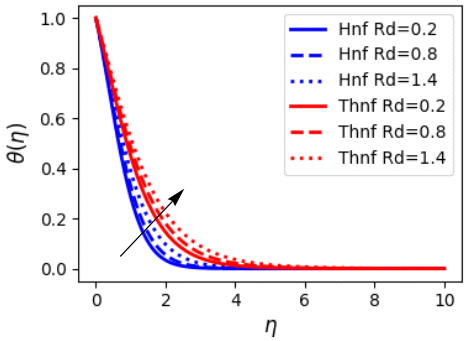

Figure 11. Influence of the radiation parameter Rd on the temperature profile $\theta(\eta)$.

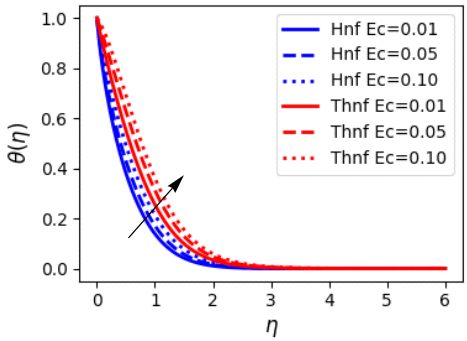

Figure 12. Influence of the Eckert number Ec on the temperature profile $\theta(\eta)$.

slowing the reaction, whereas flow unsteadiness, reduced mass diffusivity and a stronger chemical reaction lower it.

6.4 Microorganism density profile $\chi(\eta)$

The effects of the unsteadiness parameter A, bioconvection Peclet number Pe and bioconvection

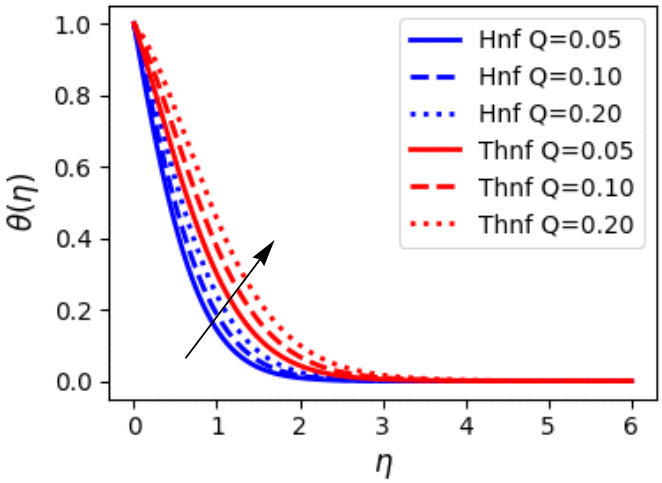

Figure 13. Influence of the heat source parameter Q on the temperature profile $\theta(\eta)$.

Schmidt number Sm on the density profile of motile microorganisms $\chi(\eta)$ are shown in Figures 18–20. The microorganism density decreases as each of the three parameters increases. A larger unsteadiness parameter increases the transient nature of the flow and leaves less time for the motile microorganisms to accumulate and diffuse into the boundary layer; as a result, the bioconvective boundary layer becomes thinner and the microorganism density distribution is reduced. Similarly, a larger Peclet number means that the directed (convective) transport of the microorganisms is more significant than their diffusive transport, so that microorganisms are removed from the vicinity of the surface at a higher rate and their density near the surface decreases. An increase in the bioconvection Schmidt number reduces the diffusivity of the motile microorganisms relative to the momentum diffusivity, which lowers their transport and hence the microorganism density profile. The results indicate that bioconvection is enhanced by a higher microorganism diffusivity, weaker flow unsteadiness and weaker convective transport.

6.5 Engineering quantities analysis

Figures 21–32 show the effect of the governing parameters on the engineering quantities, namely the skin-friction coefficient Cf_x, Nusselt number Nu_x, Sherwood number Sh_x and motile-microorganism density number Nn_x. Figures 21–23 show the effect of the Williamson parameter We, unsteadiness parameter A and magnetic parameter M on the skin-friction coefficient. The skin-friction coefficient is negative in all cases because the stretching sheet drags the fluid. It becomes more negative, i.e., its magnitude increases, as the Williamson and unsteadiness parameters increase: both parameters reduce the velocity and thin the momentum boundary layer (Figures 5 and 7), which steepens the velocity gradient at the wall. In contrast, the computed skin-friction coefficient becomes less negative, i.e., its magnitude decreases, as the magnetic parameter increases over the range $M = 0.1$–0.5.

Figures 24–26 show the influence of the unsteadiness parameter A, magnetic parameter M and radiation parameter Rd on the Nusselt number. The Nusselt number increases with the unsteadiness parameter but decreases with the magnetic and radiation parameters. Higher values of the unsteadiness parameter reduce the thickness of the thermal boundary layer, which results in a steeper temperature gradient near the wall and thus a higher rate of heat transfer. The magnetic field, on the other hand, retards the flow and heats the fluid through Joule heating, which thickens the thermal boundary layer (Figure 9) and reduces the temperature gradient at the wall, so that the Nusselt number decreases. A larger radiation parameter likewise thickens the thermal boundary layer (Figure 11) and lowers the wall temperature gradient.

The effect of the unsteadiness parameter A, Schmidt number Sc and activation energy parameter E on the Sherwood number is depicted in Figures 27–29. An increase in the unsteadiness parameter or in the activation energy reduces the Sherwood number, while an increase in the Schmidt number increases it. A larger unsteadiness parameter reduces the wall concentration gradient and hence the mass transfer. A larger activation energy slows the chemical reaction, so that less species is consumed near the wall and the wall concentration gradient decreases. As the Schmidt number increases, the mass diffusivity becomes smaller, which gives a thinner concentration boundary layer and hence a larger concentration gradient at the wall.

The impact of the unsteadiness parameter A, bioconvection Schmidt number Sm and bioconvection Peclet number Pe on the microorganism density number is shown in Figures 30–32. The microorganism density number increases with each of these parameters. Although the microorganism density inside the boundary layer decreases, the boundary layer itself becomes thinner, which results in a steeper gradient of the microorganism density at the wall and therefore a higher wall transfer rate of microorganisms.

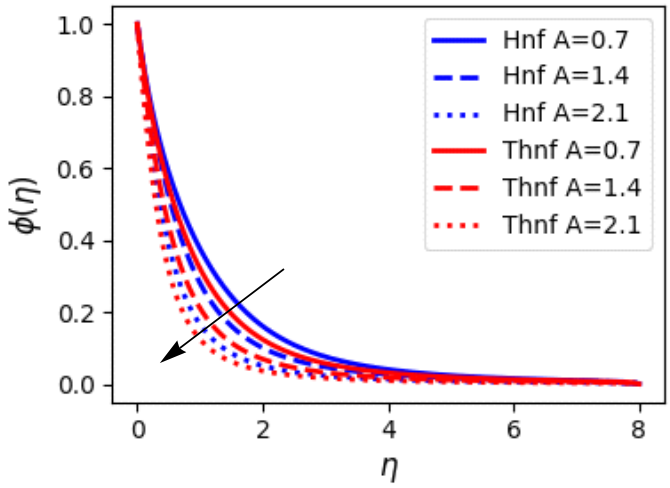

Figure 14. Influence of the unsteadiness parameter A on the concentration profile $\phi(\eta)$.

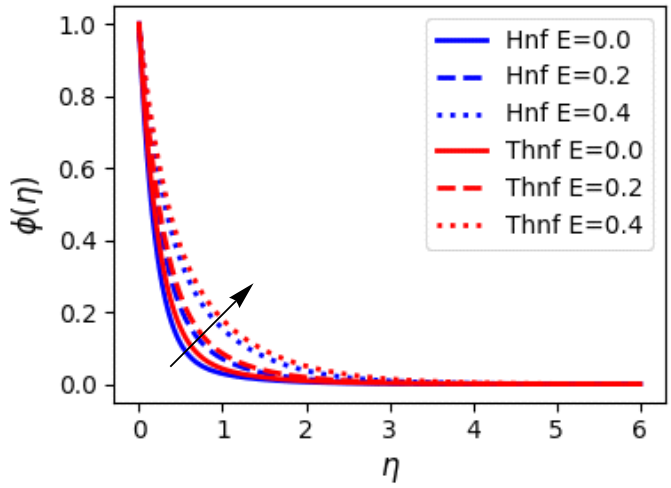

Figure 15. Influence of the activation energy parameter E on the concentration profile $\phi(\eta)$.

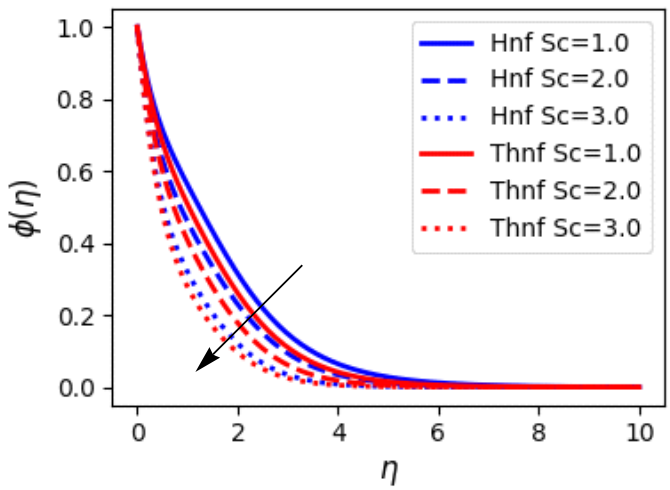

Figure 16. Influence of the Schmidt number Sc on the concentration profile $\phi(\eta)$.

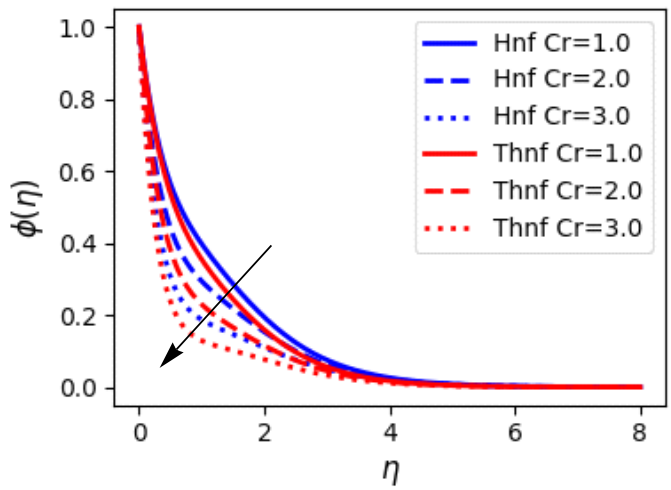

Figure 17. Influence of the chemical reaction parameter Cr on the concentration profile $\phi(\eta)$.

6.6 Artificial neural network validation

To evaluate the accuracy and reliability of the developed machine learning model, the ANN predictions are compared with the numerical results obtained from the boundary-value-problem solver, and the error distribution, training-loss history and regression behavior are examined. Figure 33 shows that the ANN predictions closely follow the numerical results, which indicates that the ANN captures the nonlinear behavior of the present Williamson tri-hybrid nanofluid. Figures 34 and 38 show the prediction error. For the concentration profile in Figure 38, the absolute error remains of the order of 10^{-6} or below over the whole computational domain (maximum 2.13×10^{-6}, mean 4.56×10^{-7}), in very good agreement with the numerical solution. The distribution of the prediction errors in Figure 37 is centered close to zero (mean -1.12×10^{-6}, standard deviation 4.37×10^{-5}, mean absolute error $\mathbf{X.XX} \times \mathbf{10^{-Y}}$, $R^2 = 0.9999987$), which indicates that the predictions are essentially unbiased. The training history in Figure 35 shows that the mean squared error remains small (of the order of 10^{-5}–10^{-4}, with intermittent spikes) over the 300 training epochs. In addition, the points in the regression plot of Figure 36 lie close to the line of perfect agreement, indicating a strong correlation between the numerical and predicted values. Overall, the validation results support the accuracy and robustness of the proposed ANN model in predicting the nonlinear solution profiles.

7 Conclusion

This study develops a comprehensive mathematical model for the unsteady magnetohydrodynamic flow of a Williamson tri-hybrid nanofluid (THNF) over a

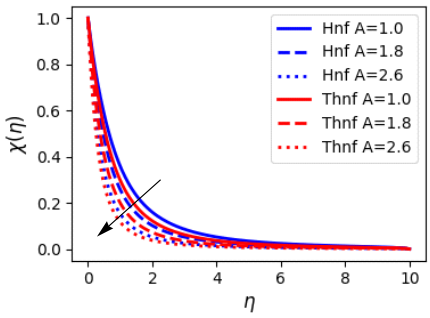

Figure 18. Influence of the unsteadiness parameter A on the microorganism profile $\chi(\eta)$.

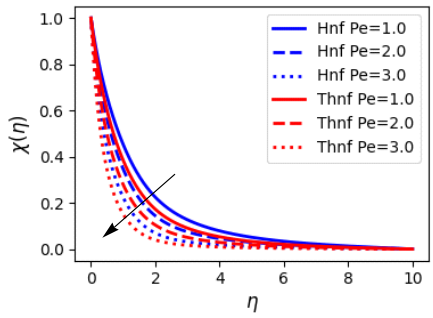

Figure 19. Influence of the bioconvection Peclet number Pe on the microorganism profile $\chi(\eta)$.

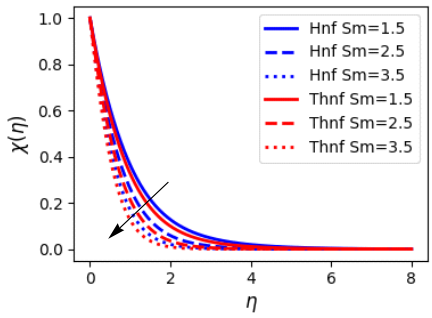

Figure 20. Influence of the bioconvection Schmidt number Sm on the microorganism profile $\chi(\eta)$.

stretching sheet in a porous medium, incorporating thermal radiation, a heat source, activation energy, chemical reaction, Brownian motion, thermophoresis and gyrotactic microorganisms. The governing equations were solved numerically and validated using a neural-network-based machine learning framework.

Scientific contributions

- To the best of the authors' knowledge, the study provides a unified framework that captures the coupled effects of unsteady Williamson rheology, a magnetic field, a porous medium, thermal radiation, activation energy and bioconvection in a tri-hybrid nanofluid system.
- The Williamson parameter and the unsteadiness parameter significantly suppress momentum transport, while the magnetic field reduces the velocity and raises the temperature.
- The activation energy parameter substantially elevates the concentration profile, highlighting its critical role in chemically reactive systems.
- The bioconvection parameters (Peclet number and bioconvection Schmidt number) directly regulate the microorganism density distribution.
- The numerical solutions and the neural network predictions are in close agreement, as shown by the regression, performance and error analyses.

Engineering implications

- The results provide flexible control strategies for thermal management through tunable parameters such as the magnetic field strength, radiation and heat source.
- They offer design guidance for applications including polymer extrusion, cooling technologies, energy systems and microfluidic transport devices.
- The Nusselt number increases with the unsteadiness parameter but decreases with the magnetic and radiation parameters, which should be taken into account when magnetic control is used in heat transfer devices.
- The Sherwood number increases with the Schmidt number and decreases with the activation energy and the unsteadiness parameter, which is relevant for reactor design.
- Once trained, the ANN surrogate can evaluate the solution profiles without repeatedly solving the boundary value problem, which makes it a promising tool for rapid parametric analysis and design optimization.

Limitations

- The model assumes an idealized flat, smooth, linearly stretching sheet and ignores surface roughness, variable fluid properties and non-uniform porosity.
- The Rosseland approximation is used for thermal radiation, which is valid only for optically thick media.
- The machine learning model is trained on a limited numerical dataset and lacks experimental validation.
- Local thermal equilibrium between the nanoparticles and the base fluid is assumed, which may oversimplify nanoscale heat transfer mechanisms.

Future developments

- Extend the model to include variable thermal conductivity and non-Darcy porous media for greater practical relevance.

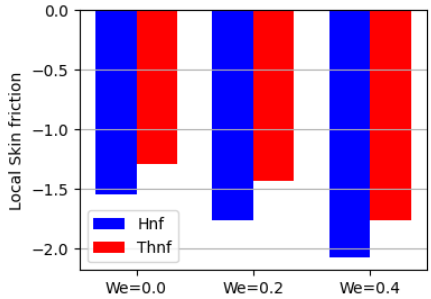

Figure 21. Influence of the Williamson parameter We on the skin friction Cf_x.

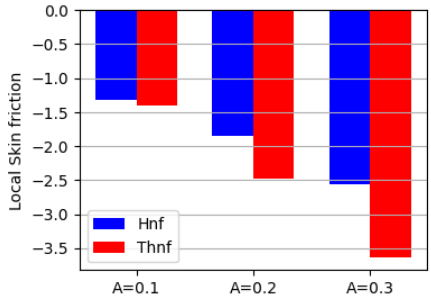

Figure 22. Influence of the unsteadiness parameter A on the skin friction Cf_x.

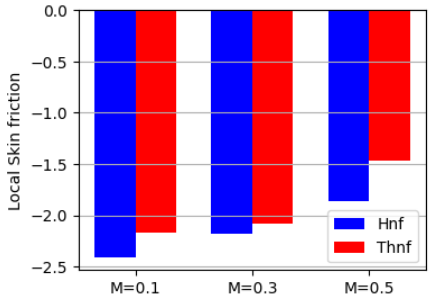

Figure 23. Influence of the magnetic parameter M on the skin friction Cf_x.

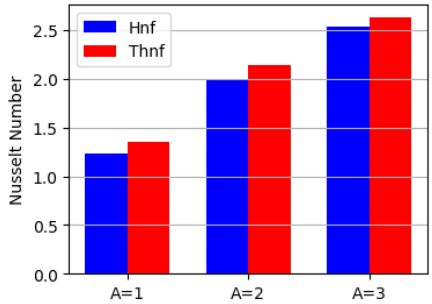

Figure 24. Influence of the unsteadiness parameter A on the Nusselt number Nu_x.

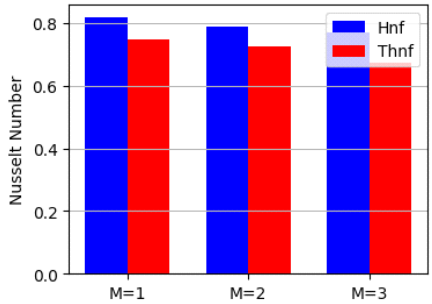

Figure 25. Influence of the magnetic parameter M on the Nusselt number Nu_x.

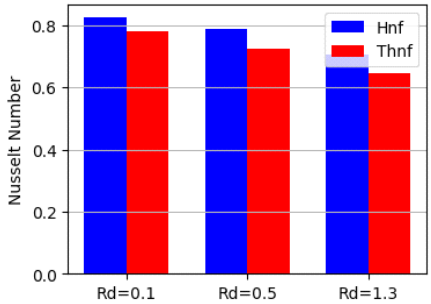

Figure 26. Influence of the radiation parameter Rd on the Nusselt number Nu_x.

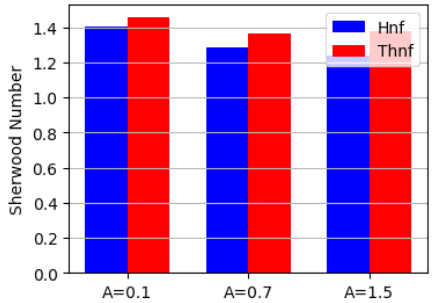

Figure 27. Influence of the unsteadiness parameter A on the Sherwood number Sh_x.

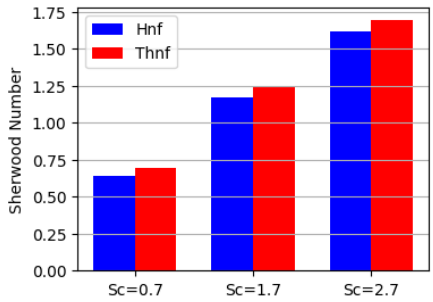

Figure 28. Influence of the Schmidt number Sc on the Sherwood number Sh_x.

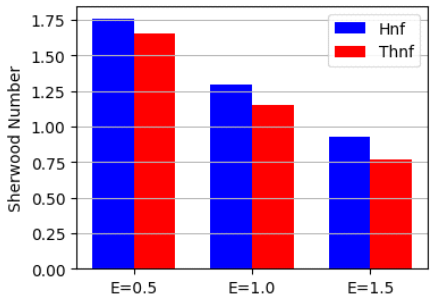

Figure 29. Influence of the activation energy parameter E on the Sherwood number Sh_x.

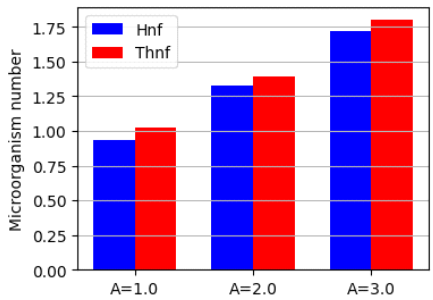

Figure 30. Influence of the unsteadiness parameter A on the microorganism density number Nn_x.

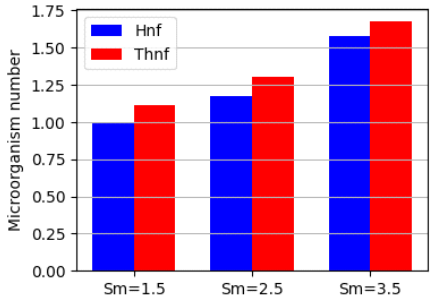

Figure 31. Influence of the bioconvection Schmidt number Sm on the microorganism density number Nn_x.

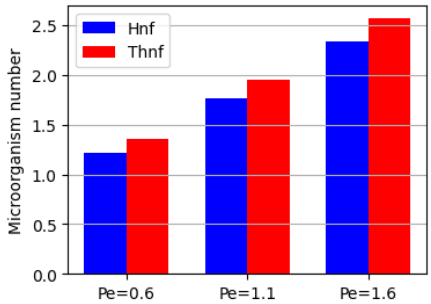

Figure 32. Influence of the bioconvection Peclet number Pe on the microorganism density number Nn_x.

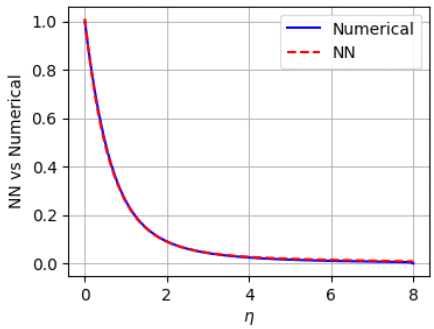

Figure 33. ANN prediction versus numerical results.

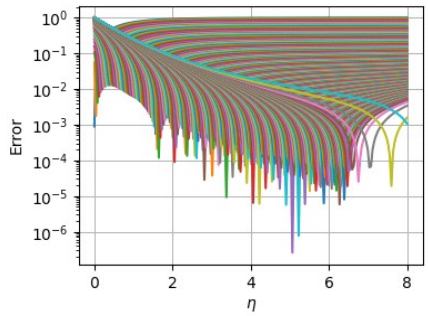

Figure 34. Error (logarithmic scale).

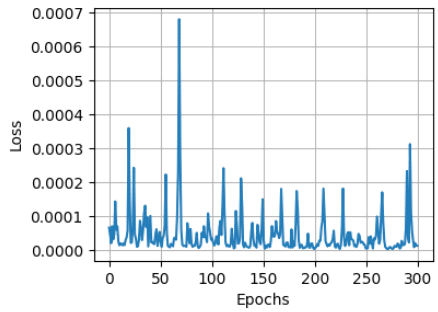

Figure 35. Training loss curve.

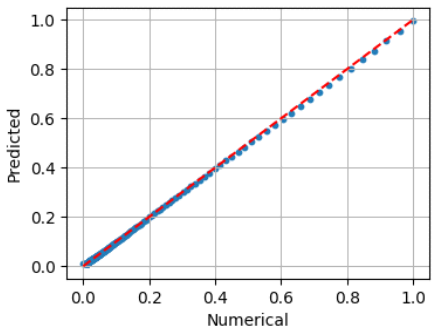

Figure 36. Regression plot.

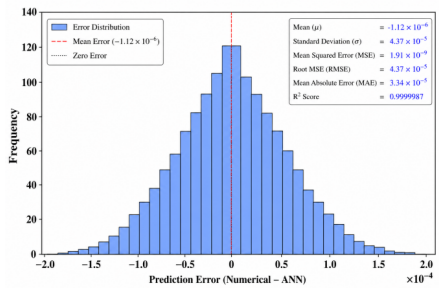

Figure 37. Histogram of the prediction errors.

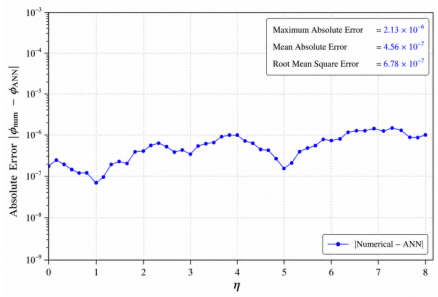

Figure 38. Absolute error between the numerical and ANN solutions.

- Conduct experimental studies to validate the numerical and machine learning predictions.
- Enhance the machine learning framework using physics-informed neural networks (PINNs) to embed the governing equations and improve generalizability.
- Explore alternative nanoparticle combinations, three-dimensional geometries and more general thermal and solutal boundary conditions.
- Incorporate uncertainty quantification and sensitivity analysis to assess the robustness of the predictions under parameter variations.

Data Availability Statement

Data will be made available on request.

Funding

This work was supported without any funding.

Conflicts of Interest

The authors declare no conflicts of interest.

AI Use Statement

The authors declare that ChatGPT was used for language editing of the manuscript. The authors have carefully reviewed, revised, and verified the AI-assisted output and take full responsibility for the content of the manuscript.

Ethical Approval and Consent to Participate

Not applicable.

References

[1] Xuan, Z., Zhai, Y., Ma, M., Li, Y., & Wang, H. (2021). Thermo-economic performance and sensitivity analysis of ternary hybrid nanofluids. *Journal of Molecular Liquids*, *323*, 114889. [CrossRef]

[2] Imran, M., Hussain, M., Jia, W., Shah, N. A., & Ali, B. (2025). Machine learning-based Bayesian regularization algorithm for thermal analysis of tri-hybrid nanofluid flow over a stretched sheet. *International Communications in Heat and Mass Transfer*, *169*, 109761. [CrossRef]

[3] Hussain, M., Lin, D., Waqas, H., Jiang, F., & Muhammad, T. (2025). Advanced thermal performance of blood-integrated tri-hybrid nanofluid: an artificial neural network-based modeling and simulation. *Mechanics of Time-Dependent Materials*, *29*(1), 16. [CrossRef]

[4] Keerthiga, M., & Reddy, P. B. A. (2025). Unsteady MHD Casson trihybrid nanofluid flow over a rotating sphere via various neural networks. *International Journal of Ambient Energy, 46*(1), 2487043. [CrossRef]

[5] Faisal, Rauf, A., Ahmad, F., & Ali Shah, N. (2025). Exploring the influence of nanolayer morphology on magnetized tri-hybrid nanofluid flow using artificial neural networks and Levenberg–Marquardt optimization. *Numerical Heat Transfer, Part B: Fundamentals, 86*(8), 2617-2639. [CrossRef]

[6] Jalili, M., Ehsani, H., Ganji, A. M., Shateri, A., Mahboobtosi, M., Wu, Y., Jalili, P., Jalili, B., & Ganji, D. D. (2025). Data-driven prediction of thermal and flow fields in magnetized Boger-micropolar tri-hybrid nanofluids via deep artificial neural networks. *Engineering Applications of Artificial Intelligence, 161*, 112232. [CrossRef]

[7] Butt, Z. I., Raja, M. A. Z., Ahmad, I., Hussain, S. I., Shoaib, M., & Ilyas, H. (2024). Radial basis kernel harmony in neural networks for the analysis of MHD Williamson nanofluid flow with thermal radiation and chemical reaction: An evolutionary approach. *Alexandria Engineering Journal, 103*, 98-120. [CrossRef]

[8] Sankari, M. S., Rao, M. E., Shams, Z. E., Algarni, S., Sharif, M. N., Alqahtani, T., ... & Irshad, K. (2024). Williamson MHD nanofluid flow via a porous exponentially stretching sheet with bioconvective fluxes. *Case Studies in Thermal Engineering, 59*, 104453. [CrossRef]

[9] Sankari, S., Rao, M. E., Elsiddieg, A. M., Khan, W., Makinde, O. D., Saidani, T., ... & Garalleh, H. A. (2025). Analytical solution of MHD bioconvection Williamson nanofluid flow over an exponentially stretching sheet with the impact of viscous dissipation and gyrotactic microorganism. *PloS one, 20*(3), e0306358. [CrossRef]

[10] Chakradhar, K., Nandagopal, K., Prashanthi, V., Parandhama, A., Somaiah, T., Thrinath, B. S., ... & Abduvalieva, D. (2025). MHD effect on peristaltic motion of Williamson fluid via porous channel with suction and injection. *Partial Differential Equations in Applied Mathematics, 13*, 101103. [CrossRef]

[11] Divya, A., Alasiri, A., Jawad, M., & Al Garalleh, H. (2025). Mixed convection and heat transfer in Williamson fluid bounded by nonlinear curved surface with heat sink/source. *Case Studies in Thermal Engineering, 73*, 106673. [CrossRef]

[12] Kumar, P., Guruprasad, M. N., Almeida, F., & Muhammad, T. (2025). Optimising the thermal characteristics of Williamson fluid flow through a microchannel influenced by the Hall effect using response surface methodology. *Case Studies in Thermal Engineering, 70*, 106139. [CrossRef]

[13] Waqas, H., Farooq, U., Muhammad, T., Hussain, S., & Khan, I. (2021). Thermal effect on bioconvection flow of Sutterby nanofluid between two rotating disks with motile microorganisms. *Case Studies in Thermal Engineering, 26*, 101136. [CrossRef]

[14] Ahmad, F., Gul, T., Khan, I., Saeed, A., Selim, M. M., Kumam, P., & Ali, I. (2021). MHD thin film flow of the Oldroyd-B fluid together with bioconvection and activation energy. *Case Studies in Thermal Engineering, 27*, 101218. [CrossRef]

[15] Ben Hamida, M. B., Irfan, M., Puthalath, A. K., & Anwar, M. S. (2025). Bioconvection behavior in radiative MHD maxwell nanofluids with gyrotactic motile microorganisms: toward enhanced solar thermal energy performance. *Journal of Thermal Analysis and Calorimetry, 150*(20), 15969-15983. [CrossRef]

[16] Madkhali, H. A., Salmi, A., Alharbi, S. O., & Alqahtani, A. S. (2026). Impact of hybrid nanoparticles on heat and mass transfer in the presence of movement of motile gyrotactic microorganisms. *Waves in Random and Complex Media, 35*(7), 13262-13280. [CrossRef]

[17] Arif, U., & Nawaz, M. (2025). Numerical study of motile gyrotactic micro-organisms in hybrid nano-Maxwell fluid with mass and heat transfer. *Waves in Random and Complex Media, 35*(7), 13501-13517. [CrossRef]

[18] Sarma, A. K., & Sarma, D. (2026). Unsteady magnetohydrodynamic bioconvection Casson fluid flow in presence of gyrotactic microorganisms over a vertically stretched sheet. *Numerical Heat Transfer, Part A: Applications, 87*(1), 2389338. [CrossRef]

[19] Hussain, M., Shahid, S., Akbar, N. S., & Alaoui, M. K. (2025). Unsteady flow and heat transfer optimization of viscous fluid with bioconvection over a rotating stretchable disk and gyrotactic motile microorganisms. *Case Studies in Thermal Engineering, 66*, 105796. [CrossRef]

[20] Panda, S., Ontela, S., Mishra, S. R., & Thumma, T. (2024). Effect of Arrhenius activation energy on two-phase nanofluid flow and heat transport inside a circular segment with convective boundary conditions: Optimization and sensitivity analysis. *International Journal of Modern Physics B, 38*(25), 2450342. [CrossRef]

[21] Raju, U., Rangabashyam, S., Alhazmi, H., & Khan, I. (2024). Irreversible and reversible chemical reaction impacts on convective Maxwell fluid flow over a porous media with activation energy. *Case Studies in Thermal Engineering, 61*, 104821. [CrossRef]

[22] Varatharaj, K., Tamizharasi, R., & Vajravelu, K. (2024). Carreau nanofluid dynamics with activation energy gyrotactic microorganisms in a porous medium: Application to solar energy. *International Journal of Thermofluids, 24*, 100823. [CrossRef]

[23] Ullah, H., Abas, S. A., Fiza, M., Jan, A. U., Akgul, A., Abd El-Rahman, M., & Al-Mekhlafi, S. M. (2025). Thermal radiation effects of ternary hybrid nanofluid flow in the activation energy: Numerical computational approach. *Results in Engineering, 25*,

104062. [CrossRef]

[24] Anwar, T., Ullah, K., Fiza, M., Ullah, H., Mahariq, I., & Al Mekhlafi, S. M. (2025). Recurrent neural network approach to thermal radiation in hybrid nanofluids with activation energy between two rotating disks. *Results in Physics, 77*, 108451. [CrossRef]

[25] Ayman-Mursaleen, M., Saeed, S. T., Almohammadi, S. M., Arif, K., & Imran, M. (2026). A deep neural network model for heat transfer in Darcy–Forchheimer hybrid nanofluid flow with activation energy. *Scientific Reports, 16*(1), 8339. [CrossRef]

[26] Rehman, A., Inc, M., Saad, A. A., Abas, S. S., Sudarmozhi, K., & Khashi'ie, N. S. (2026). Thermal radiation and viscous dissipation impact on 2D MHD Williamson ternary hybrid nanofluid flow over a stretching surface. *Discover Nano, 21*(1), 211. [CrossRef]

[27] Raptis, A. (1998). Radiation and free convection flow through a porous medium. *International Communications in Heat and Mass Transfer, 25*(2), 289-295. [CrossRef]

[28] Ouyang, Y., Md Basir, M. F., Naganthran, K., & Pop, I. (2024). Triple solutions for unsteady stagnation flow of tri-hybrid nanofluid with heat generation/absorption in a porous medium. *Case Studies in Thermal Engineering, 61*, 105027. [CrossRef]

[29] Guedri, K., Khan, A., Sene, N., Raizah, Z., Saeed, A., & Galal, A. M. (2022). Thermal flow for radiative ternary hybrid nanofluid over nonlinear stretching sheet subject to Darcy–Forchheimer phenomenon. *Mathematical Problems in Engineering, 2022*(1), 3429439. [CrossRef]

Abdul Hafeez received his M.Phil. degree in Mathematics in 2025 from the Department of Mathematics, The Islamia University of Bahawalpur, Pakistan. His research interests include fluid mechanics, heat and mass transfer, nanofluid and hybrid nanofluid flows, boundary layer theory, and mathematical modeling. (Email: f23bmath3e01035@iub.edu.pk)

Javed Khan is a Ph.D. student at the School of Mathematics and Computational Science, Xiangtan University, Hunan, China. He holds an M.Phil. degree in Mathematics from Quaid-i-Azam University, Islamabad, Pakistan, and an M.Sc. in Mathematics from Abdul Wali Khan University Mardan, KP, Pakistan. His research interests include algebraic cryptography, algebraic coding theory, and fluid mechanics. (Email: 202561510001@smail.xtu.edu.cn)

Xiao Ying is a master's student in Computational Mathematics at the School of Mathematics and Computational Science, Xiangtan University, Hunan, China. She holds a bachelor's degree in Mathematics and Applied Mathematics from Huaihua University. Her primary research interests focus on the numerical solution of partial differential equations. (Email: 202521511246@smail.xtu.edu.cn)